This is a preprint, the final version is subject to change, of the American Mineralogist (MSA)
Cite as Authors (Year) Title. American Mineralogist, in press.
DOI: https://doi.org/10.2138/am-2018-6531

# Revision 1

# Surface energy of fayalite and its effect on Fe-Si-O oxygen buffers and the olivine-spinel transition

Kristina Lilova[1], Michael T. DeAngelis[2], Lawrence M. Anovitz[3], Alexandra Navrotsky[1]

[1]Peter A. Rock Thermochemistry Laboratory and NEAT ORU, University of California Davis, Davis, California 95616
[2]University of Arkansas at Little Rock, Earth Sciences Little Rock AR, 72204-1099
[3]Geochemistry and Interfacial Sciences Group, Oak Ridge National Laboratory, Oak Ridge, TN 37831-6110

## Abstract

The surface energy (hydrated surfaces) of fayalite ($\alpha$-$Fe_2SiO_4$) was determined to be 2.47 ± 0.25 J/m$^2$ using high temperature oxide melt solution calorimetry. This is larger than the surface energy of magnetite ($Fe_3O_4$), but lower than that of forsterite ($\alpha$-$Mg_2SiO_4$). The changes in the positions of the quartz/fayalite/magnetite (QFM) and quartz/iron/fayalite (QIF) buffers with particle size reduction were calculated. QFM is lowered in $fO_2$ by 3-7 log units as a function of temperature for 30 nm particles while QIF is raised by 1-2 log units. The estimated surface energy difference between olivine and spinel polymorphs decreases the pressure of the olivine-spinel transition in $Fe_2SiO_4$ by about 1 GPa.

## INTRODUCTION

Oxidation - reduction equilibria of nanoscale iron oxides have been shown to depend significantly on particle size because the phases involved have different surface energies (Navrotsky et al. 2010). Although surface energies have been measured for hematite, maghemite - magnetite solid solutions, and ulvospinel (Majzlan et al. 2003; Lilova et al. 2014), few experimental data are available for silicates. Because fayalite ($\alpha$-$Fe_2SiO_4$) is an important component of the rock-forming olivines, and is involved in a number of "redox buffers" that define oxygen fugacity in synthetic and petrologic systems, including important extraterrestrial materials, and participates in high pressure phase transitions, its surface energy is needed to understand the behavior of these reactions when small particles are involved. In addition, because there has been significant discussion of olivines as mantle water reservoirs (Férot and Bolfan-Casanova 2012), this work determines the enthalpy of the hydrated fayalite surface using high temperature oxide melt solution calorimetry of one bulk and several nanophase fayalite samples.

# EXPERIMENTAL PROCEDURES

## Materials

Several samples of fayalite were analyzed in this experiment. Powdered nanophase samples, indicated as fayalite FS21, 22, 23, 24, and 26, were used as received from Michael DeAngelis. A sample of bulk fayalite was prepared by Donald Lindsley (5-15-17 fayalite). The synthesis of the nanophase fayalite was described in detail by DeAngelis et al. (2012). The bulk $Fe_2SiO_4$ (5-15-17 fayalite) was prepared by mixing silica and $Fe_2O_3$ and grinding them together for 2 hours under ethanol in an agate mortar. "Fe-sponge" was then added and ground for an additional 40 minutes. The mix was wrapped in silver foil and inserted into a silica-glass tube, which was evacuated and sealed, then annealed in a furnace at 930–940 °C for 10 days. X-ray diffraction (XRD) showed that the product was ~97 % fayalite, ~1.4 % quartz, ~1.3 % wüstite, and ~0.5% metallic Fe. This material was then re-ground and annealed for 15 days to react the small amount of silica, wüstite, and Fe to fayalite. A third heating was performed with additional Fe-sponge due to a small leak that caused a partial oxidation of one end of the sample during the second run. This was run for about 45 days, XRD of the final product showed ~1 % free quartz, ~99 % fayalite, with no unreacted wüstite. Optical examination in refractive index oil confirmed the presence of quartz; other than a few globules of silver, there were no opaque particles, strongly suggesting the absence of hematite, wüstite, magnetite, and metallic Fe. Absence of the latter two was further confirmed by testing with a magnet, to which no sample adhered.

## Characterization

The amount of surface water on each of the nano-sized samples was determined by simultaneous thermogravimetry and differential scanning calorimetry (TG-DSC). Each fayalite sample was heated in argon from room temperature to 1073 K at 10 K/min in a Setaram Labsys Evo instrument.

X-ray diffraction (XRD) of the bulk sample was performed on a Rigaku Miniflex 600, using Cu Kα radiation. Data were processed with Match! 3$^{TM}$ software, and the unit-cell parameters were determined by Rietveld refinement using FullProf$^{TM}$. The characterization of the nano fayalite samples was described in detail by DeAngelis et al. (2012).

## Calorimetry

High temperature oxide melt solution calorimetry was performed using the Setaram AlexSYS - the commercial version of the Tian Calvet twin calorimeter described previously by Navrotsky (1977, 1997, 2014). In the drop solution calorimetry experiment, samples in the form of pellets (between 4 and 6 mg) were dropped from room temperature (298 K) into molten $2PbO{\cdot}B_2O_3$ solvent at 1073 K in a platinum crucible. Pure oxygen was flushed through the system and bubbled through the solvent at 110 and 5 ml/min, respectively, to remove the evolved water vapor and assist in the complete oxidation of $Fe^{2+}$ to $Fe^{3+}$. More details about the reproducible final oxidation state of Fe-containing compounds dissolved in lead borate can be found in Lilova et al. (2012).

# RESULTS

## Characterization

The XRD of the bulk sample showed fayalite ($a$ = 4.815, $b$ = 10.468, $c$ = 6.084 Å) with about 1 % free silica as quartz. According to DeAngelis et al. (2012), the nano fayalite samples contain 3 wt. % or less metallic Fe (0.6 wt. % for FS22). The weight loss from the thermogravimetric analysis corresponds to the total water content (physisorbed and chemisorbed) on the surface of the sample. While it is possible that simultaneous weight gain may have occurred due to oxidation, the product was checked by XRD after the TGA measurement and found to be a coarsened fayalite.

## Enthalpy of formation and surface enthalpy of fayalite

The calorimetric data for the six samples analyzed in this study are given in Table 1. The enthalpy of formation of bulk fayalite from oxides at 298 K is calculated as -25.91 ± 2.42 kJ/mol, using the thermodynamic cycle shown in Table 2. Calculation of the enthalpy of formation of all samples, however, requires that the measured drop solution enthalpies be corrected for the water and the small amount of Fe reported in the nano fayalite, and the silica in the bulk one (Table 1). The 3 wt.% of Fe reported in the nanophase $Fe_2SiO_4$ sample would result in a change of approximately -36 kJ/mol. This is a significant change relative to the values measured for each sample. For example, the drop solution enthalpy of sample FS23 is –38.63 kJ/mol. If FS23 contains 3 wt % Fe, $\Delta H_{ds}$ becomes -2.66 kJ/mol. After the water correction, the final drop solution enthalpy would be -47 kJ/mol, which is practically the drop solution enthalpy of bulk fayalite (Table 3), i.e. the nanophase compound would appear to be as thermodynamically stable as its bulk counterpart. It should be noted, however, that FS23 has the smallest particle size. Similar calculations performed for FS21 would result in a drop solution enthalpy of -38 kJ/mol after all corrections, which would indicate higher energetic stability for the nano fayalite than the bulk one. In fact, any Fe content above or equal to 1 wt % would result in drop solution enthalpies more endothermic than -48.15 kJ/mol for at least one of the nano fayalite. This seems unreasonable and we, therefore, conclude that the Fe content in these nano samples is likely to be significantly less than 3 % and may be closer to the value found for FS22 (0.6 wt %) (DeAngelis et al., 2012). Hence all drop solution enthalpies for the nano samples have been corrected for 0.6 wt% Fe. Similarly, the drop solution enthalpy of bulk fayalite was corrected for 1 wt % quartz. We realize that the nanophase fayalite samples have compositional uncertainties but realistically, better samples cannot be readily prepared at present. Though the cumulative errors arising from iron content, water content, and possible sample heterogeneity cannot be rigorously quantified, the data, as the first experimental measurement of fayalite surface energy, are new and useful.

To compare the results from this study with reported values for fayalite the values must also be corrected for the composition of wüstite, as the enthalpy of formation from the oxides should be to end-member FeO. The enthalpy of the reaction $0.106Fe + 2Fe_{0.947}O = 2FeO$ is -7.11 ± 5.39 kJ/mol (Robie and Hemingway 1995). The drop solution enthalpy of pure Fe in lead borate solvent at 1073 K was calculated using the thermodynamic cycle in Table 4. Correcting the measured values to an enthalpy of formation of fayalite from stoichiometric FeO and $SiO_2$

then yields -18.80 ± 5.91 kJ/mol. This is reasonably consistent with values from the literature (-17.2 ± 6.3 kJ/mol, Thierry et al. 1981; -20.5 kJ/mol, Hewitt 1978; -24.6 ± 2.1 kJ/mol, Robie et al. 1978).

The corrected drop solution enthalpies of all fayalite samples as a function of surface area are shown on Figure 1. The data have been fitted to a straight line, the absolute value of the slope of which, 2.47 ± 0.25 J/m$^2$, is equal to the surface energy. The error is two standard deviations of the slope. Because the correction for water content was made using the heat content of pure $H_2O$, neglecting any interactions of water with the surface, this energy refers to that of the hydrated surface, as discussed previously (Ushakov et al. 2005). Water adsorption calorimetry on the nano fayalite samples would be needed to make appropriate corrections to obtain the enthalpy of the anhydrous surface. Unfortunately, insufficient material was available for such studies.

For all the calculations below, we have used the reported surface energies of the hydrated surfaces for consistency. This is reasonable, as nanoparticles hold on strongly to their surface water and its total removal often coincides with coarsening (Navrotsky, 2011). Thus, calculation of phase equilibria under most laboratory and natural conditions where nanoparticles occur generally should be done using the energetics of the hydrated surfaces.

## DISCUSSION

### Oxygen buffers at the nanoscale

Oxygen buffers are used to control or estimate the oxygen fugacity of synthetic and natural systems. Several of these, such as magnetite/hematite, quartz/fayalite/magnetite, magnetite/wüstite, and wüstite/iron are based on oxidation - reduction reactions involving metallic, divalent and trivalent Fe. It is possible that the phases involved may have small particle sizes and thus the differences in surface energies between the bulk and nano-phases may shift the redox equilibria (Navrotsky et al. 2010), especially at low to moderate temperatures, where recrystallization/crystal growth are less likely, or in cases of shear or fault zones (Krot et al. 2000; Sammis and Ben-Zion 2008),

In order to evaluate the importance of nanoparticle size on fayalite-bearing redox buffers, we have calculated the positions of the quartz/fayalite/magnetite and quartz/iron/fayalite buffers

$$3Fe_2SiO_4 + O_2 \rightarrow 2Fe_3O_4 + 3SiO_2 \quad \text{QFM} \quad (1)$$

$$2Fe + SiO_2 + O_2 \rightarrow Fe_2SiO_4 \quad \text{QIF} \quad (2)$$

for 100, 50, and 30 nm diameter particles. The fayalite/wüstite buffers were not assessed, because $Fe_{1-x}O$ nanoparticles are not thermodynamically stable below around 1000 K, and at such temperatures it is likely wüstite will coarsen (Navrotsky et al. 2010). This limitation, combined with the non-stoichiometry of wüstite complicates the calculations and significantly increases the uncertainty.

The oxygen fugacities of the bulk and nano QFM buffers were calculated for reaction 1 using eqs. 4 – 6.

$$\log p_{O_2} = \frac{\Delta G_r}{2.3RT} \quad (4)$$

$$\log p_{O_2} = \frac{\Delta G_r + \Delta G_r^{ex}}{2.3RT} \quad (5)$$

$$\Delta G_r^{ex} = 2(\Delta H_{surface}, Fe_3O_4) + 3(\Delta H_{surface}, SiO_2) - 3(\Delta H_{surface}, Fe_2SiO_4) \quad (6)$$

where $\Delta G_r$ is the Gibbs free energy of the bulk QFM reaction, $\Delta G_r^{ex}$ is the excess Gibbs free energy associated with the nano QFM reaction, and $\Delta H_{surface}$ is the total enthalpy of the surface of each phase, i.e the surface enthalpy times the surface area per mole of phase corresponding to the given particle size. Analogous formulae were used for the QIF buffer with the respective coefficients. All values are shown in Tables 5 and 6, and the results of the calculations are shown in Figures 2-3. The results for the bulk redox buffers between 300 and 900 K are consistent with the data of Misra (2012). The results suggest that decreases in fayalite particle size significantly destabilize it, decreasing the oxygen fugacity of the QFM buffer and favoring the stability of magnetite (Fig. 2). The calculated shift in QFM is 3-7 log units for the smallest particle size (30 nm), depending on temperature. The effect on the oxygen fugacity of the QIF buffer (Fig. 3) is to increase its oxygen fugacity, again destabilizing fayalite to a small extent although, since the amount of oxygen in the QIF reaction is smaller than in QFM (equations 1 and 2) the effect is smaller. Thus, we conclude that the QFM buffer is more sensitive to particle size effects than QIF.

**High pressure olivine - spinel phase transition**

Mantle olivines are predominantly composed of forsterite, but also contain a significant fayalite component (Ringwood 1975; Irifune and Isshiki 1998). The olivine/spinel transition is a well-known feature of the mantle (Hart 1969; Ringwood 1970). It includes the two transitions at the Mg-rich end (forsterite to wadsleyite and wadsleyite to ringwoodite) and the one transition at the Fe-rich end (fayalite to ahrensite).

The surface enthalpy (hydrated surface) of fayalite (2.47 J/m$^2$) is higher than that of typical Fe spinels (0.80 J/m$^2$ for magnetite and ulvospinel, Lilova et al. 2012a, 2012b), and smaller than that of the hydrous forsterite surface (3.37 J/m$^2$, Chen et al. 2009). If the surface enthalpy of ahrensite γ-$Fe_2SiO_4$ is similar to that of other Fe-bearing spinels, this difference between fayalite and spinel will result in thermodynamic stabilization of the spinel relative to the olivine, which will, thereforer, reduce the pressure of the Fe-rich olivine-spinel transition for small particle sizes. To estimate the effect of this difference on the pressure of the phase transition, the following approximate calculation was performed.

$$P = \frac{T\Delta S - \Delta H}{\Delta V_m} \quad (8)$$

where P, ΔS, ΔH, $\Delta V_m$ are the pressure, entropy, enthalpy, and molar volume of the transition. The effects of thermal expansion and compressibility were neglected, and the enthalpy, entropy, and volume of the transition were assumed constant for illustrative purposes, as our goal is to estimate the magnitude of the pressure change resulting from the decrease in particle size, not to

make an accurate calculation of the equilibrium pressure. Assuming 2.47 J/m$^2$ surface energy (hydrated surface) for fayalite and 0.8 J/m$^2$ (the same as for magnetite) for ahrensite ($\gamma$-$Fe_2SiO_4$), for a particle size of 100 nm, the enthalpy of the transition from $\alpha$-$Fe_2SiO_4$ (fayalite) to $\gamma$-$Fe_2SiO_4$ (ahrensite) decreases by about 5 kJ/mol, yielding a pressure drop of approximately 1 GPa. Since the equilibrium pressure for this transition near 1273 K is around 6 GPa (Akaogi et al. 1989) this represents a drop of about 17 %, which is outside the error of pressure calibrations and may be significant. While the expected temperature of this transition is large enough that nanoparticles are likely to recrystallize, diminution of particle size during shearing or as a consequence of phase transition (Riedel and Karato 1997; Jackson 2000; Michibayashi et al. 2006) could generate such effects. This pressure drop is comparable, on a percentage basis, to that calculated for the forsterite – wadsleyite transition in $Mg_2SiO_4$ calculated by Chen and Navrotsky (2010), who measured the surface enthalpy of forsterite for both hydrated and anhydrous surfaces by a combination of oxide melt solution calorimetry and water adsorption calorimetry. They then calculated the change in the transition pressure for the forsterite - wadsleyite transition assuming that $\beta$-$Mg_2SiO_4$ has a surface enthalpy similar to that of $MgAl_2O_4$ spinel. For an average grain size of 100 nm, 4.4 J/m$^2$ surface energy for the olivine and 1.8 J/m$^2$ for the $\beta$-$Mg_2SiO_4$, the calculated transition pressure was lowered by about 2 GPa (above 19 %) and the transition enthalpy by around 7 kJ/mol. Again, particle size reduction favors the high pressure phase, which has the lower surface enthalpy. If ringwoodite and wadsleyite have similar surface energies, both being spinel-related structures, then the $\beta$–$\gamma$ transition should be much less affected by particle size reduction than the $\alpha$–$\beta$ transition.

There are no experimental data available for the surface energy of olivine, wadsleyite, or ringwoodite solid solutions with Mg/(Mg+Fe) near 0.9, which is characteristic of mantle olivines. Near that composition, the high pressure transitions are solid solution loops in the $\alpha$+$\beta$ and $\beta$+$\gamma$ fields. The assumptions made by Chen and Navrotsky (2010) in calculating the forsterite - wadsleyite transition in $Mg_2SiO_4$ can, however, be generalized to the solid solutions. One can reasonably assume that in the olivine phase the surface energy varies linearly between those of forsterite and fayalite. Unfortunately, there are few constraints on the surface energies of wadsleyite and ringwoodite solid solutions. Nonetheless, within the framework of the assumptions made by Chen and Navrotsky (2010), one can perform very approximate calculations suggesting that, within rather large uncertainties, particle size diminution to 100 nm would lower the pressure of first appearance of wadsleyite for an olivine of Mg/(Mg+Fe) = 0.9 by about 2 GPa, similar to that for pure $Mg_2SiO_4$.

## IMPLICATIONS

The surface energy of fayalite ($\alpha$-$Fe_2SiO_4$) is significantly higher than that of magnetite ($FeFe_2O_4$) and other spinels, including, presumably, ahrensite $\gamma$-$Fe_2SiO_4$. Thus, Fe-bearing spinel phases are thermodynamically stabilized relative to fayalite at the nanoscale. This difference in surface energy causes a significant shift in the quartz/fayalite/magnetite (QFM) buffer to lower oxygen fugacity and the $Fe_2SiO_4$ olivine-spinel transition to lower pressure. The quartz/iron/fayalite (QIF) buffer is less affected. Thus, under petrologic regimes where fine particles are likely to form and persist (e.g. sedimentary and low grade metamorphic conditions, high strain rates, phase transition induced grain size diminution), one must be cautious in

applying established oxygen buffers and geobarometers/geothermometers to estimate conditions of phase assemblage formation. For particle sizes below 100 nm, corrections of several orders of magnitude in oxygen fugacity and 1-2 GPa in pressure may be required. In addition, particle-size-driven local shifts in the oxygen fugacity of the QFM buffer could be relevant to redox-related processes in the mantle transition zone such as mid-ocean ridge basalt glass melting and crystallization, element partitioning, and volcanic degassing. As the oxidized to total Fe ratio is expected to be a function of particle size this can affect the bulk composition and geophysical properties and of the mineral assemblage, and thus related geologic processes.

## ACKNOWLEDGEMENTS

This material is based upon work supported by the U.S. Department of Energy, Office of Science, Office of Basic Energy Sciences, Chemical Sciences, Geosciences, and Biosciences Division (calorimetry at UC Davis was supported under Award number DE-FG02ER1474). Work by MTD was conducted at the Center for Nanophase Materials Sciences, which is a DOE Office of Science User Facility. The authors thank D.H. Lindsley for careful synthesis of the bulk 5-15-17 fayalite sample.

## REFERENCES

Akaogi, M., Ito, E., and Navrotsky, A. (1989) Olivine-Modified Spinel-Spinel transitions in the system $Mg_2SiO_4$ - $Fe_2SiO_4$: Calorimetric measurements, thermochemical calculation, and geophysical application. Journal of Geophysical Research, 94, 15671–15685.

Bina, C.R., and Wood, B.J. (1987) Olivine-Spinel Transitions: Experimental and Thermodynamic Constraints and Implications for the Nature of' the 400-km Seismic Discontinuity, Journal of Geophysical Research, 92, 4853-4866.

Chen, S., and Navrotsky A. (2010) Calorimetric study of the surface energy of forsterite. American Mineralogist, 95, 112–117.

DeAngelis, M.T., Rondinone, A.J., Pawel, M. D., Labotka, T.C., and Anovitz L.M. (2012) Sol-gel synthesis of nanocrystalline fayalite ($Fe_2SiO_4$). American Mineralogist, 97, 653–656.

Férot A., and Bolfan-Casanova N. (2012) Water storage capacity in olivine and pyroxene to 14 GPa: Implications for the water content of the Earth's upper mantle and nature of seismic discontinuities. Earth and Planetary Science Letters, 349–350, 218-230.

Hart P. J. (1969) International upper mantle project. Sci. Rep. 21 1708, Washington DC, AGU

Hemingway B.S. (1990) Thermodynamic properties for bunsenite, NiO, magnetite, $Fe_3O_4$, and hematite, $Fe_2O_3$, with comments on selected oxygen buffer reactions. American Mineralogist, 75, 781-790.

Hewitt D.A. (1978) A redetermination of the fayalite-magnetite-quartz equilibrium between 650 degrees and 850 degrees C. American Journal of Science, 278, 715-724.

Jacob, K.T., Kale, G.M., and Iyengar, G.N.K. (1989) Chemical potentials of oxygen for fayalite-quartz-lron and fayalite-quartz-magnetite equilibria. Metallurgical and Materials Transactions B 20B, 679-685.

Jackson, I. (2000) The Earth's Mantle: Composition, Structure, and Evolution, Cambridge University Press, 594 pages

Irifune T., and Isshiki M. (1998) Iron partitioning in a pyrolite mantle and the nature of the 410-km seismic discontinuity. Nature, 392, 702-705.

Krot, A.N., Brearley, A.J., Petaev, M.I., Kallemeyn, G.W., Sears, D.W.G., Benoit, P.H., Hutcheon, I.D., Zolensky, M.E., and Keil, K. (2000) Evidence for low-temperature growth of fayalite and hedenbergite in MacAlpine Hills 88107, an ungrouped carbonaceous chondrite related to the CM-CO clan. Meteoritics and Planetary Science, 35, 1365-1386.

Lilova, K.I., Xu, F., Rosso, K.M., Pearce, C.I., Kamali, S., and Navrotsky, A. (2012a) Oxide melt solution calorimetry of $Fe^{2+}$-bearing oxides and application to the magnetite–maghemite ($Fe_3O_4$–$Fe_{8/3}O_4$) system. American Mineralogist, 97, 164 – 175.

Lilova, K.I., Pearce, C.I., Gorski, C., Rosso, K.M., and Navrotsky, A. (2012b) Thermodynamics of the magnetite-ulvöspinel ($Fe_3O_4$-$Fe_2TiO_4$) solid solution. American Mineralogist, 97, 1330-1338.

Lilova, K.I., Pearce, C.I., Rosso, K M., and Navrotsky, A. (2014) Energetics of Spinels in the Fe-Ti-O System at the Nanoscale. A European Journal of Chemical Physics and Physical Chemistry, 15, 3655–3662.

Majzlan, J., Lang, B.E., Stevens, R., Navrotsky, A., Woodfield, B. F., and Boerio-Goates J. (2003) Thermodynamic properties, low-temperature heat-capacity anomalies, and single-crystal X-ray refinement of hydronium jarosite, $(H_3O)Fe_3(SO_4)2(OH)6$. American Mineralogist, 88, 846-854.

Michibayashi, K., Ina, T. and Kanagawa K. (2006) The effect of dynamic recrystallization on olivine fabric and seismic anisotropy: Insight from a ductile shear zone, Oman ophiolite. Earth Planet Science Letters, 244, 695-708.

Misra, K. (2012) Introduction to Geochemistry: Principles and Applications. John Wiley & Sons

Navrotsky, A. (1977) Progress and new directions in high temperature calorimetry. Physics and Chemistry of Minerals, 2, 89–104.

Navrotsky, A. (1997) Progress and new directions in high–temperature calorimetry revisited. Physics and Chemistry of Minerals, 24, 222–241.

Navrotsky, A., Dorogova, M., Hellman, F., Cooke, D.W., Zink, B. L., Lesher, C.E., Boerio-Goates, J., Woodfield, B.F., and Lang, B. (2007) PNAS, 104, 9187–9191.

Navrotsky, A., Ma, C., Lilova, K., and Birkner, N. (2010) Nanophase transition metal oxides show large thermodynamically driven shifts in oxidation-reduction equilibria. Science, 330, 199-201.

Navrotsky, A. (2011) Nanoscale Effects on Thermodynamics and Phase Equilibria in Oxide Systems. A European Journal of Chemical Physics and Physical Chemistry, 12, 2207 – 2215.

Navrotsky, A. (2014) Progress and New Directions in Calorimetry: A 2014 Perspective. Journal of the American Ceramic Society, 97, 3349-3359.

Parks, G.A. (1990) Mineral-Water Interface Geochemistry, Reviews in Mineralogy, 23, 133–176.

Riedel, M.R., and Karato S. (1997) Grain-size evolution in subducted oceanic lithosphere associated with the olivine–spinel transformation and its effects on rheology. Earth Planet Science Letters, 148, 27–43.

Ringwood, A.E. (1970) Phase transformations and the constitution of the mantle. Physics of the Earth and Planetary Interiors, 9, 109-155.

Ringwood, A.E. (1975) Composition and Petrology of the Earth's Mantle, McGraw-Hill, New York.

Robie, R.A., Hemingway, B.S., and Fisher J.R. (1978) Thermodynamic properties of minerals and related substances at 298.15 K and 1 Bar (105 Pascals) pressure and at higher Termperatures. US Geological Survey Bulletin, 1452, Washington

Robie, R.A., and Hemingway, B.S. (1995) Thermodynamic properties of minerals and related substances at 298.15 K and 1 bar (10^5 pascals) pressure and at higher temperatures. US Geological Survey Bulletin, 2131, Washington

Sammis, C.G., and Ben-Zion, Y. (2008) Mechanics of grain-size reduction in fault zones. Journal of Geophysical Research, 113, B02306.

Syono, Y., Tokonami, M., and Matsui Y. (1971) Crystal field effect on the olivine-spinel transformation. Physics of the Earth and Planetary Interiors, 4, 347-352.

Thierry, P., Chatillon-Colinet, C., Mathieu, J.C., Regnard, J.R., and Amosse, J. (1981) Thermodynamic properties of the forsterite-fayalite ($Mg_2SiO_4$-$Fe_2SiO_4$) solid solution. determination of heat of formation. **Physics and Chemistry of Minerals**, 7, 43-46.

S. Ushakov, and A. Navrotsky (2005) Direct measurements of water adsorption enthalpy on hafnia and zirconia. Applied Physics Letters, 87, 164103.

414 **Fig. 1.** Corrected drop solution enthalpy of five nanophase and one bulk fayalite samples fitted
415 as a linear function of the surface area with $R^2 = 0.997$. The fit yields a surface energy of the
416 hydrated surface of $2.47 \pm 0.25$ J/m$^2$
417 **Fig. 2.** QFM buffer curve change with particle size. The nano curves are calculated for 100, 50,
418 and 30 nm particle diameter with data for hydrated surfaces.
419 **Fig. 3**. QIF buffer curve change with particle size. The nano curves are calculated for 100, 50,
420 and 30 nm particle diameter with data for hydrated surfaces.
421

This is a preprint, the final version is subject to change, of the American Mineralogist (MSA)
Cite as Authors (Year) Title. American Mineralogist, in press.
DOI: https://doi.org/10.2138/am-2018-6531

**Table 1.** Calorimetric data for all fayalite samples. The drop solution enthalpies are corrected for impurities and total water content as discussed in the text. Reported errors are two standard deviations of the mean, (n) is number of experiments performed.

| Sample | BET area $m^2$/mol | Particle size, calculated from BET, nm | $\Delta H_{ds}$ kJ/mol | $\Delta H_{ds}$ kJ/mol, corrected for water and impurities |
|---|---|---|---|---|
| bulk | 0 | >1000 | –47.19 ± 0.92(8) | –48.15 ± 0.95 |
| FS22 | 2568 | 108 | –54.71 ± 1.72(8) | –51.79 ± 1.73 |
| FS21 | 4320 | 64 | –50.85 ± 0.82(8) | –63.51 ± 0.84 |
| FS24 | 5456 | 50 | –45.56 ± 2.03(9) | –66.27 ± 2.04 |
| FS26 | 5616 | 49 | –45.28 ±1.36(12) | –67.24 ± 1.37 |
| FS23 | 9577 | 29 | –38.63 ± 1.30(12) | –72.91 ± 1.32 |

**Table 2.** Thermodynamic cycle for calculating enthalpy of formation of fayalite

| | |
|---|---|
| $Fe_2SiO_4$ (s, 298 K) + 0.5$O_2$ (g, 1073 K) → $Fe_2O_3$ (dis, 1073K) + $SiO_2$ (dis, 1073K) | $\Delta H_{ds}$ |
| Fe (s, 298 K) + 0.75$O_2$ (g, 1073 K) → 0.5$Fe_2O_3$ (dis, 1073 K) | $\Delta H_2$ |
| $O_2$ (g, 298 K) → $O_2$ (g, 1073 K) | $\Delta H_3$ |
| $Fe_{0.947}O$ (s, 298 K) + 0.21025 $O_2$ (g, 1073 K) → 0.4735 $Fe_2O_3$ (dis, 1073 K) | $\Delta H_5$ |
| $SiO_2$ (s, 298 K) → $SiO_2$ (dis, 1073 K) | $\Delta H_6$ |
| **0.106Fe (s, 298 K) + 2$Fe_{0.947}O$ (s, 298 K) + $SiO_2$ (s, 298 K) → $Fe_2SiO_4$ (s, 298 K)** $\Delta H_{f,ox} = -\Gamma H_{ds} + 0.106\Gamma H_2 + 2\Gamma H_5 + \Gamma H_6$ | |

**Table 3** Iron, wüstite, magnetite and hematite drop solution enthalpies ($\Delta H_{ds}$) in lead borate, 1073 K.

| Sample | $\Delta H_{ds}$ [kJ/mol] | $\Delta H_{ox}$ [kJ/mol] | $\Delta H_{f,el}$ [kJ/mol] |
|---|---|---|---|
| Fe | –344.21 ± 4.44 (calculated) | -830.51 ± 4.53 | 0 |
| $Fe_{0.947}O$ | –42.68 ± 1.08[1] | –124.17 ± 1.25 | –268.49 ± 1.70 |
| $Fe_3O_4$ | 147.58 ± 1.12[1] | –120.37 ± 2.30 | –1124.20 ± 4.30 |
| α–$Fe_2O_3$ | 182.29 ± 1.34[1] | 0 | –829.70 ± 2.42 |
| quartz $SiO_2$ | 47.79 ± 0.32[2] | 0 | –910.7 ± 1 |

[1]Lilova et al., 2012
[2]Navrotsky, 2014

**Table 4**. Thermodynamic cycle for calculating enthalpy of drop solution of iron metal in lead borate at 1073 K.

This is a preprint, the final version is subject to change, of the American Mineralogist (MSA)
Cite as Authors (Year) Title. American Mineralogist, in press.
DOI: https://doi.org/10.2138/am-2018-6531

| | |
|---|---|
| **$Fe_3O_4$ (s, 298 K) + 0.25$O_2$ (g, 1073 K) → 1.5 $Fe_2O_3$ (dis, 1073 K)** | $\Delta H_1$ |
| Fe (s, 298 K) + 0.75$O_2$ (g, 1073 K) → 0.5$Fe_2O_3$ (dis, 1073 K) | $\Delta H_2$ |
| $O_2$ (g, 298 K) → $O_2$ (g, 1073 K) | $\Delta H_3$ |
| | |
| **3Fe (s, 298 K) + 2$O_2$ (g, 298 K) → $Fe_3O_4$ (s, 298 K)** | $\Delta H_4$ |
| $\Delta H_4 = -\Delta H_1 + 2*\Delta H_3 + 3*\Delta H_2$ | |

**Table 5.** Gibbs free energies of the bulk and nano buffer reactions. The Gibbs energies of the bulk reaction are calculated using the Gibbs energies of formation from Robie et al. (1978), Hemingway (1990), and Jacob et al. (1989). The excess Gibbs energies for the nano reaction are calculated using the surface energies from Lilova et al. (2012), Navrotsky et al. (2010) and this work. The excess Gibbs energy is assumed equal to the excess enthalpy as obtained from the surface energy differences, as done previously (Navrotsky et al., 2010).

| Reaction | $\Delta G_r$, kJ/mol | $\Gamma G_r^{ex}$ 100 nm, kJ/mol | $\Gamma G_r^{ex}$ 50 nm, kJ/mol | $\Gamma G_r^{ex}$, 30 nm kJ/mol |
|---|---|---|---|---|
| QFM buffer | -530.82 + 0.22T ± 3.52 | -12.24 ± 2.13 | -24.47 ± 4.24 | -40.79 ± 7.07 |
| QIF buffer | -565.36 + 0.14T ± 1.62 | 4.16 ± 0.74 | 8.33 ± 1.47 | 13.88 ± 2.44 |

**Table 6.** The surface enthalpies and surface areas of all phases (hydrated surface) for 100, 50, and 30 nm particle diameter

| Phase | Surface energy, $J/m^2$ | Surface area for 100 nm, $m^2/mol$ | Surface area for 50 nm, $m^2/mol$ | Surface area for 30 nm, $m^2/mol$ | $\Delta H_{surface}$, 100 nm kJ/mol | $\Delta H_{surface}$, 50 nm kJ/mol | $\Delta H_{surface}$, 30 nm kJ/mol |
|---|---|---|---|---|---|---|---|
| Fe | 1.59±0.22[1] | 426 | 851 | 1418 | 0.68±0.09 | 1.35±0.19 | 2.25±0.31 |
| $Fe_3O_4$ | 0.80±0.05[2] | 2697 | 5395 | 8992 | 2.16±0.13 | 4.32±0.27 | 7.19±0.45 |
| $Fe_2O_3$ | 0.75±0.16[1] | 1808 | 3616 | 6026 | 1.36±0.29 | 2.71±0.58 | 4.52±0.96 |
| $SiO_2$ | 1.0±0.1[3] | 1361 | 2723 | 4538 | 1.36±0.14 | 2.72±0.27 | 4.54±0.45 |
| $Fe_2SiO_4$ | 2.47±0.25 | 27850 | 5570 | 9283 | 6.88±0.7 | 13.76±1.39 | 22.93±2.32 |

[1]Navrotsky et al., 2010
[2]Lilova et al., 2012
[3]Parks 1990

This is a preprint, the final version is subject to change, of the American Mineralogist (MSA)
Cite as Authors (Year) Title. American Mineralogist, in press.
DOI: https://doi.org/10.2138/am-2018-6531

Figure 1

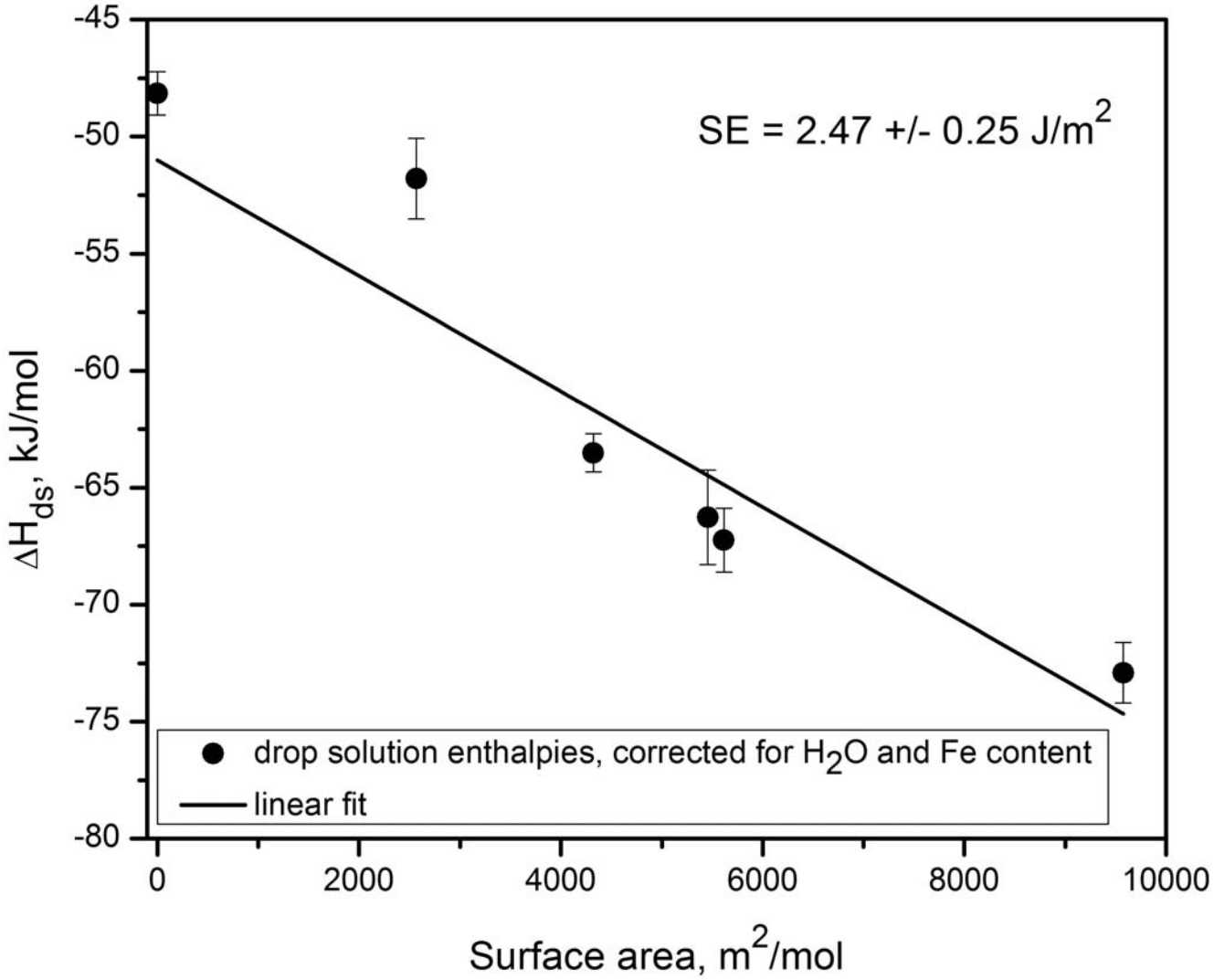

This is a preprint, the final version is subject to change, of the American Mineralogist (MSA)
Cite as Authors (Year) Title. American Mineralogist, in press.
DOI: https://doi.org/10.2138/am-2018-6531

Figure 2

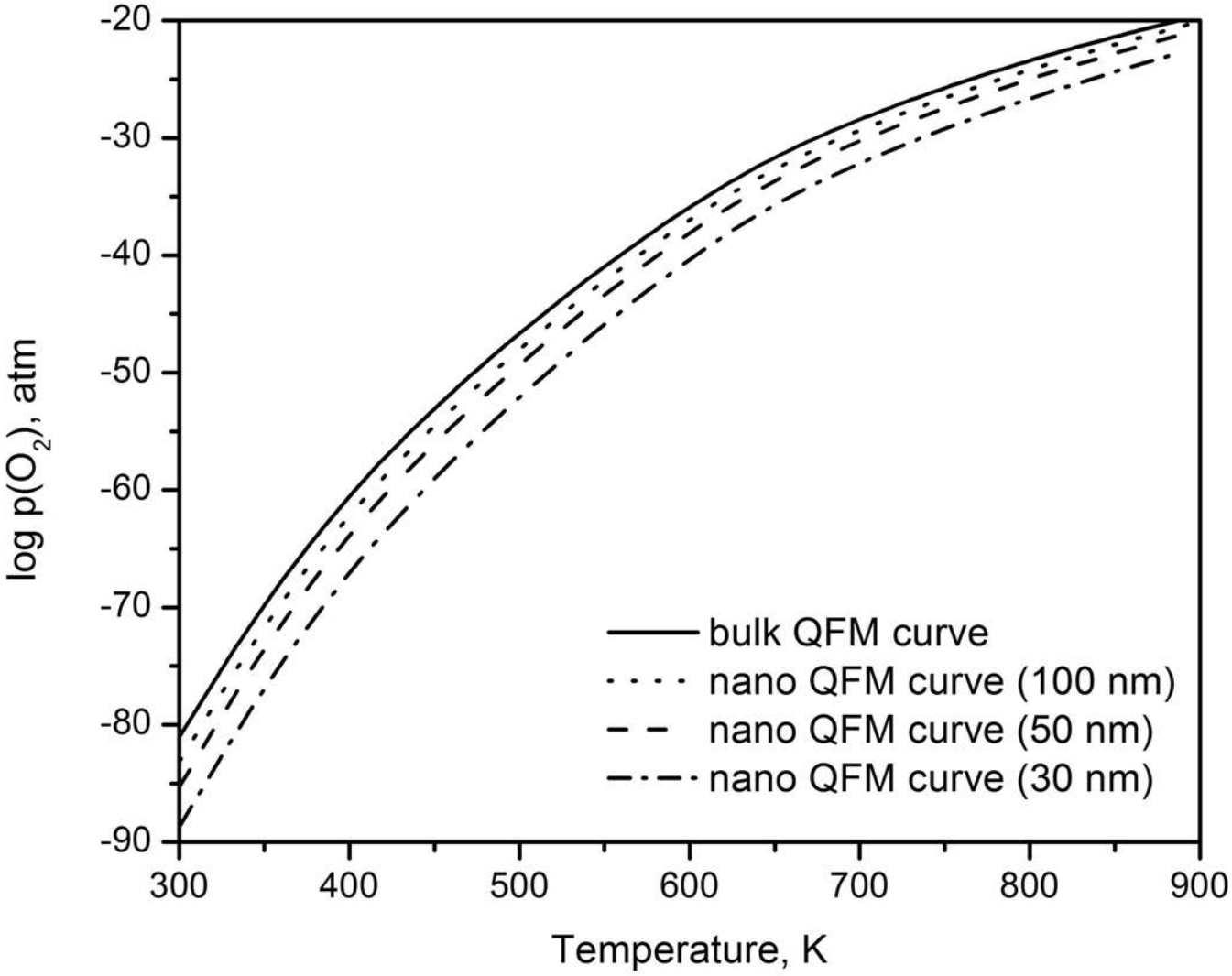

This is a preprint, the final version is subject to change, of the American Mineralogist (MSA)
Cite as Authors (Year) Title. American Mineralogist, in press.
DOI: https://doi.org/10.2138/am-2018-6531

Figure 3